ORGANOMETALLICS
Article

Organometallics **2010,** *29,* 4251–4264 4251
DOI: 10.1021/om1002478

Rare, Hexatomic, Boat-Shaped, Cross-Linked Bis(iminodiphenylphosphorano)methanediide Pincer Carbon Bridged Photoluminescent Copper Clusters Capped with Methyl or Halide Bridges

Guibin Ma,[†] Michael J. Ferguson,[‡] Robert McDonald,[‡] and Ronald G. Cavell*,[†]

[†]*Department of Chemistry and* [‡]*X-ray Structure Determination Laboratory, University of Alberta, Edmonton, Alberta T6G 2G2, Canada*

Received March 30, 2010

The dimeric dilithium methanediide salt $[Li_2C(Ph_2P{=}NSiMe_3)_2]_2$ ($[Li_2L]_2$, L = $[C(Ph_2P{=}NSiMe_3)_2]^{2-}$) reacted with 6 equiv of $[NEt_4CuCl_2]$ and 2 equiv of LiMe in THF or ether to give exclusively the six-copper cluster complex $[Cu_6L_2(CH_3)_2]$ (**1**). Similarly, $[Li_2L]_2$ reacted with 3 equiv of the bimetallic copper halide complexes $[(cod)_2Cu_2X_2]$ (X = Cl, Br, I) in the same solvent to give good yields of three halide-capped six-copper clusters $[Cu_6L_2(X)_2]$ (X = Cl (**2**), Br (**3**), I (**4**)) with structures very similar to that of **1**. These four hexacopper clusters (**1**−**4**) as a family show similar ^{31}P NMR spectra with an AB pattern with slightly different chemical shifts but identical coupling constants in solution. The reactivity of **2** was explored, and it was demonstrated that **1** can be quantitatively generated by addition of 2 equiv of LiMe to **2**. Moreover, the cluster $[Cu_6L_2(O^tBu)_2]$ (**5**) with a similar cage structure is quantitatively generated by reaction of **2** with 2 equiv of NaO^tBu in solution according to ^{31}P NMR spectroscopy. An additional copper complex with a bicopper formulation, $[Cu_2L(PPh_3)_2]$ (**6**), was synthesized by reaction of $[Li_2L]_2$ with 2 equiv of $[(NEt_4)Cu(PPh_3)Cl_2]$. We also observed a monocopper iodide complex with the doubly protonated parent methylene bridged ligand H_2L, $[CuI(H_2L)]$ (**7**), as a minor component (about 10%) during the preparation of complex **4**. Complexes **1**−**4**, **6**, and **7** were characterized by X-ray crystal diffraction. All four clusters (**1**−**4**) show a rare boat-shaped conformation of hexacopper clusters assembled by cross-linking of two copper atoms via geminal substitution on one bis(iminophosphorano)methanediide ligand. Two of these units combine along with two additional copper atoms to form the boat cluster. There is extensive direct Cu−Cu bonding. The cluster is doubly capped, top and bottom, by methyl groups (**1**) or halides (**2**−**4,** X = Cl, Br, I). All of these six-copper clusters absorb and emit in the UV−vis region. The absorption bands and photoluminescent wavelengths are substituent dependent; thus, optical properties of the complex are tunable by means of substitution of the capping ligands. The spectral and bonding characteristics were explored by means of Gaussian DFT calculations and NBO analysis.

Introduction

The design and synthesis of unique d^{10} metal copper(I) complexes in either monomeric or polynuclear forms with subsequent exploration of their photophysical properties and applications for selected catalysis functions continues to be an active research area.[1] A large variety of possible metal−metal and metal−ligand bonding combinations can be assembled, often creating interesting and sometimes unique chemical properties. In addition, some luminescent polynuclear Cu(I) carbon bound compounds with a variety of bridged ligands have been extensively reported.[2] Current interest centers on photoluminescence properties which offer potential for applications in photovoltaic and optoelectronic devices. Several previous studies have reported polynuclear copper(I) clusters constructed with tetrahedral cores, octahedral cores, or bridging ligands based on group 15 or 16 elements.[3] A few examples of copper(I) clusters with alkynyl ligands are also known.[4] To the best of our knowledge, there are no known copper clusters supported by bridging carbon centers or carbon-bound pincer chelate ligands.

We have used the dilithiated bis(diphenyltrimethylsilyl-iminophosphorano)methanediide salt $[Li_2L]_2$ (or the parent methylene ligand H_2L) in our laboratory to synthesize both monomeric and bimetallic bridged carbon metal complexes.[5] Particularly successful were the unique spirocyclic bimetallics[6a,b] of Pd(II) and Rh(I) (Scheme 1). In addition, we recently reported a spirocyclic dimetalated carbon Tl(I) complex of this same ligand which dimerized to a tetrathallated cluster through the formation of Tl(I)−Tl(I) bonds.[6c] Herein we report a set of copper(I) hexatomic metal clusters with a unique, irregular

*To whom correspondence should be addressed. Tel: 780-492-5310. Fax: 780-492-8231. E-mail: ron.cavell@ualberta.ca.

(1) (a) Ohishi, T.; Nishiura, M.; Hou, Z.-M. *Angew. Chem., Int. Ed.* **2008**, *47*, 5792–5795. (b) Badiei, Y. M.; Dinescu, A.; Dai, X.-L.; Palomino, R. M.; Heinemann, F. W.; Cundari, T. R.; Warren, T. H. *Angew. Chem., Int. Ed.* **2008**, *47*, 9961–9964. (c) Badiei, Y. M.; Krishnaswamy, A.; Melzer, M. M.; Warren, T. H. *J. Am. Chem. Soc.* **2006**, *128*, 15056–15057. (d) Zhang, X.-M.; Fang, R.-Q.; Wu, H.-S. *J. Am. Chem. Soc.* **2005**, *127*, 7670–7671. (e) Xie, H.-Y.; Kinoshita, I.; Karasawa, T.; Kimura, K.; Nishioka, T.; Akai, I.; Kanemoto, K. *J. Phys. Chem. B* **2005**, *109*, 9339–9345. (f) Che, C.-M.; Mao, Z.; Miskowski, V. M.; Tse, M.-C.; Chan, C.-K.; Cheung, K.-K.; Phillips, D. L.; Leung, K.-H. *Angew. Chem., Int. Ed.* **2000**, *39*, 4084–4088.

Published on Web 09/07/2010

Scheme 1. Hetero- and Homobimetallic Spirocyclic Complexes of Bis(diphenyltrimethylsilyliminophosphorano)methanediide and a Tl(I) Dimeric Cluster of the Spirocyclic Complex of the Same Ligand

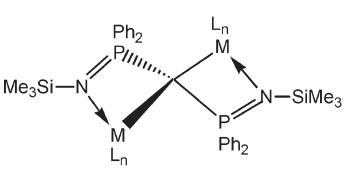

M = Pd and Rh, (L_n = CO, allyl or cod)

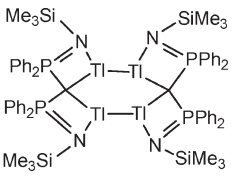

Tl Tetramer

structural arrangement formed from an unusual ligating structure. These complexes also show unusual and potentially useful optical behavior.

Results and Discussion

We prepared the copper(I) clusters $[Cu_6L_2X_2]$ ($L = C(Ph_2P{=}NSiMe_3)_2^{2-}$; $X = CH_3^-$ (**1**), Cl^- (**2**), Br^- (**3**), I^- (**4**)) by reacting the appropriate Cu(I) precursors (either $CuCl_2^-$ salts plus MeLi or $Cu_2(cod)X_2$ (X = Cl, Br, I) with the organodilithium dimer $[Li_2C(Ph_2P{=}NSiMe_3)_2]_2$, ($[Li_2L]_2$) in either THF or ether solutions (Scheme 2). ^{31}P NMR spectra of all these copper clusters in solution show an AB coupling pattern with slightly different ^{31}P chemical shifts, indicating nearly chemically identical but magnetically inequivalent P atoms within the pincer ligand. The AB coupling constants were deduced by simulation of the experimental spectra; the parameters for all are almost identical (Table 1). All four complexes were structurally characterized.

Scheme 2. Preparation of Complexes 1−4

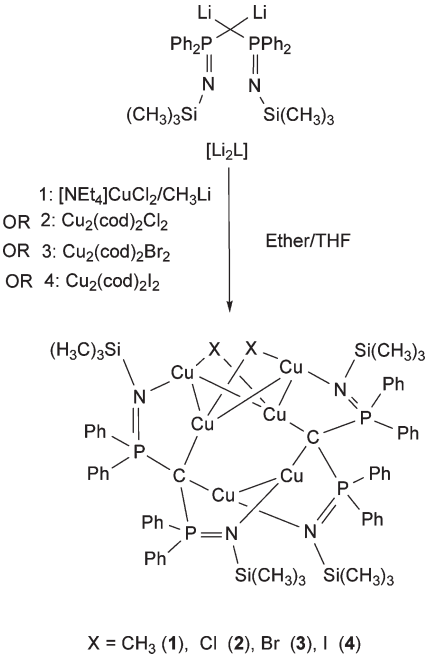

X = CH_3 (**1**), Cl (**2**), Br (**3**), I (**4**)

Table 1. ^{31}P NMR Chemical Shifts and Spin−Spin Coupling Constants for Compounds 1−5

compd[a]	P_A (ppm)	P_B (ppm)	J_{A-B} (Hz)	solvent
$Cu_6L_2(CH_3)_2$ (**1**)	25.14	24.33	58	toluene
$Cu_6L_2(Cl)_2$ (**2**)	28.24	26.17	56	THF
$Cu_6L_2(Br)_2$ (**3**)	28.10	26.59	57	THF
$Cu_6L_2(I)_2$ (**4**)	28.95	28.08	56	THF
$Cu_6L_2(O^tBu)_2$ (**5**)	27.58	23.95	62	THF

[a] $L = [C\{Ph_2P{=}NSi(CH_3)_3\}_2^{2-}]$.

A monocopper complex of the (iminophosphorano)methine ligand system, $[\{CH(PPh_2N{=}SiMe_3)_2\}CuPPh_3]$, has recently been reported.[7] It was synthesized by the reaction of potassium bis(iminophosphono)methanide with $[(Ph_3P)_2CuI]$. The crystal structure shows that the carbon is not directly bonded to the copper atom in this complex but, rather, shows the existence of a weak ionic pair interaction. We have successfully prepared a related bimetallic copper complex of the methanediide $[Cu_2L(PPh_3)_2]$ ($L = C(Ph_2P{=}NSiMe_3)_2^{2-}$) (**6**) in situ by reacting $[NEt_4][Cu(PPh_3)Cl_2]$ with $[Li_2L]_2$ in THF. The ^{31}P NMR spectrum of **6** shows one broad peak at 4.06 ppm and one doublet peak at 19.34 ppm with a P−P coupling constant of 5 Hz, differing from the data for the previously reported complex, indicating that a new compound has formed in the solution. This new complex was isolated and structurally characterized (see below).

It is interesting to note that when we prepared cluster **4** with a reaction stoichiometry of six Cu metals to 1 mol of the ligand salt, $[Li_2L]_2$, complex $[CuI(H_2L)]$ (**7**) was formed in

(2) (a) Yam, V. W.-W.; Lo, K. K.-W. *Chem. Soc. Rev.* **1999**, 323–334. (b) Yam, V. W.-W.; Lo, K. K.-W. *J. Chem. Soc., Dalton Trans.* **1995**, 499–500. (c) Yam, V. W.-W.; Chan, L.-P.; Lai, T.-F. *J. Chem. Soc., Dalton Trans.* **1993**, 2075–2077. (d) Yam, V. W.-W.; Lee, W.-K.; Cheung, K.-K. *J. Chem. Soc., Dalton Trans.* **1996**, 2335–2339. (e) Jarvis, J. A. J.; Pearce, R.; Lappert, M. F. *J. Chem. Soc., Dalton Trans.* **1977**, 999–1003. (f) Yam, V. W.-W.; Choi, S. W.-K.; Chan, C.-L.; Cheung, K.-K. *Chem. Commun.* **1996**, 2067–2068. (g) Yam, V. W.-W.; Cheng, E. C.-C.; Zhu, N.-Y. *Chem. Commun.* **2001**, 1028–1029. (h) Yam, V. W.-W.; Lam, C.-H.; Cheung, K.-K. *Chem. Commun.* **2001**, 545–546. (i) Yam, V. W.-W.; Fung, W. K.-M. *Chem. Commun.* **1998**, 777–778. (j) Yam, V. W.-W.; Fung, W. K.-M.; Cheung, K.-K. *Chem. Commun.* **1997**, 963–964. (k) Knotter, D. M.; Smeets, W. J. J.; Spek, A. L.; Van Koten, G. *J. Am. Chem. Soc.* **1990**, *112*, 5895–5896. (l) He, X.-M.; Ruhlandt-Senge, K.; Power, P. P.; Bertz, S. H. *J. Am. Chem. Soc.* **1994**, *116*, 6963–6964. (m) Olmstead, M. M.; Power, P. P. *J. Am. Chem. Soc.* **1990**, *112*, 8008–8014. (n) Knotter, D. M.; Spek, A. L.; van Koten, G. *J. Chem. Soc., Chem. Commun.* **1989**, 1738–1740. (o) Wehman, E.; van Koten, G.; Erkamp, C. J. M.; Knotter, D. M.; Jastrzebski, J. T. B. H.; Stam, C. H. *Organometallics* **1989**, *8*, 94–99. (p) Lenders, B.; Grove, D. M.; van Koten, G.; Smeets, W. J. J.; van der Sluis, P.; Spek, A. L. *Organometallics* **1991**, *10*, 786–791. (q) Aalten, H. L.; van Koten, G.; Riethorst, E.; Stam, C. H. *Inorg. Chem.* **1989**, *28*, 4140–4146. (r) Guss, M.; Mason, R.; Søtofte, I.; van Koten, G.; Noltes, J. G. *J. Chem. Soc., Chem. Commun.* **1972**, 446–447. (s) Chan, W.-H.; Zhang, Z.-Z.; Mak, T. C. W.; Che, C.-M. *J. Organomet. Chem.* **1998**, *556*, 169–172. (t) Koshevoy, I. O.; Karttunen, A. J.; Tunik, S. P.; Haukka, M.; Selivanov, S. I.; Melnikov, A. S.; Serdobintsev, P. Y.; Khodorkovskiy, M. A.; Pakkanen, T. A. *Inorg. Chem.* **2008**, *47*, 9478–9488.

(3) (a) Drew, M. G. B.; Lavery, A.; McKee, V.; Nelson, S. M. *J. Chem. Soc., Dalton Trans.* **1985**, 1771–1774. (b) Liu, C. W.; Hung, C.-M.; Santra, B. K.; Wang, J.-C.; Kao, H.-M.; Lin, Z.-Y. *Inorg. Chem.* **2003**, *42*, 8551–8556. (c) Ohlmann, D.; Pritzkow, H.; Grutzmacher, H.; Anthamatten, M.; Glaser, R. *J. Chem. Soc., Dalton Trans.* **1995**, 1011–1012. (d) Eichhöfer, A.; Fenske, D.; Holstein, W. *Angew. Chem., Int. Ed.* **1993**, *32*, 242–245. (e) Fenske, D.; Steck, J.-C. *Angew. Chem., Int. Ed.* **1993**, *32*, 238–242. (f) Vogler, A.; Kunkely, H. *J. Am. Chem. Soc.* **1986**, *108*, 7211–7212. (g) Kutal, C. *Coord. Chem. Rev.* **1990**, *99*, 213–252.

(4) (a) Olbrich, F.; Kopf, J.; Weiss, E. *Angew. Chem., Int. Ed.* **1993**, *32*, 1077–1079. (b) ten Hoedt, R. W. M.; Noltes, J. G.; van Koten, G.; Spek, A. L. *J. Chem. Soc., Dalton Trans.* **1978**, 1800–1806.

(5) (a) Cavell, R. G.; Babu, R. P. K.; Aparna, K. *J. Organomet. Chem.* **2001**, *617*, 158–169. (b) Jones, N. D.; Cavell, R. G. *J. Organomet. Chem* **2005**, *690*, 5485–5496. (c) Cavell, R. G. In *The Chemistry of Pincer Compounds*; Morales-Morales, D., Jensen. C. M., Eds.; Elsevier: Amsterdam, 2007; Chapter 14, pp311−346 and references therein.

(6) (a) Fang, M.; Jones, N. D.; Friesen, K.; Lin, G.-Y.; Ferguson, M. J.; McDonald, R.; Lukowski, R.; Cavell, R. G. *Organometallics* **2009**, *28*, 1652–1665. (b) Ma, G.-B.; McDonald, R.; Cavell, R. G. *Organometallics* **2010**, *29*, 52–60. (c) Ma, G.-B.; Ferguson, M. J.; Cavell, R. G. *Chem. Commun.* **2010**, 5370–5372.

(7) Panda, T. K.; Roesky, P. W.; Larsen, P.; Zhang, S.; Wickleder, C. *Inorg. Chem.* **2006**, *45*, 7503–7508.

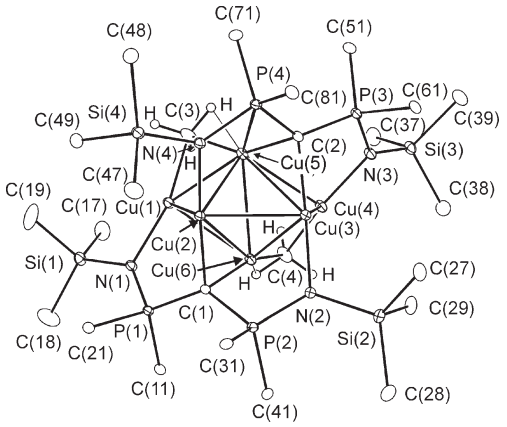

Figure 1. Perspective view of complex **1** showing the atom-labeling scheme. Only the ipso carbons of the phenyl groups are shown. Hydrogen atoms (except for those of the bridging methyl groups) are omitted. Non-hydrogen atoms are represented by Gaussian ellipsoids at the 20% probability level. Bond lengths and angles are given in Table 2.

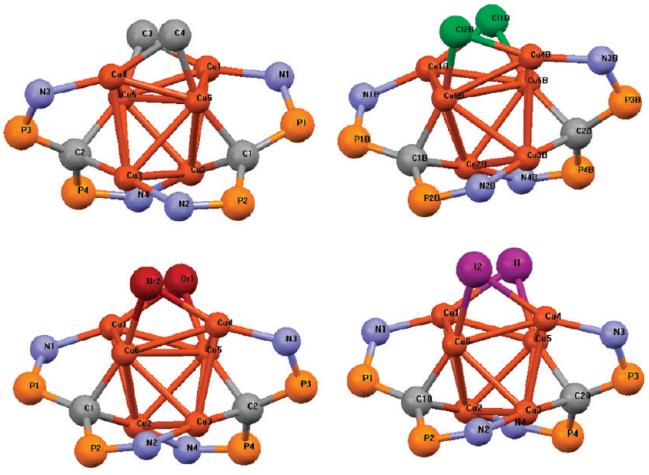

Figure 2. Core structures of copper(I) clusters **1** (top left), **2** (top right), **3** (bottom left), and **4** (bottom right). For selected bond distances (Å) and angles (deg), see Table 2.

situ in approximately 10% concentration along with **4** on the basis of solution ^{31}P NMR. That solution produced two differently colored crystals, light green ([CuI(H_2L)] (**7**)) and red ([$Cu_6I_2L_2$] (**4**)). Increasing the copper ratio to 10:1 yielded **7** as the major product, which was readily isolated for crystal structure analysis (see below).

Crystals of all four cluster complexes (**1**−**4**) were obtained either from ether or mixed ether/THF solutions. All are bright yellow or golden orange. Crystal structures have been determined for all, and they show a unique structural geometry. The structure of **1** (which is representative of **1**−**4**) is shown in Figure 1, and the central cluster core structures of all four are illustrated in Figure 2. The common feature of the structures is provided by geminally binding two copper atoms to the central carbon of a methanediide (N═P−C^{2-}−P═N) ligand. One of these geminal Cu(I) atoms in each unit is then coordinated to a nitrogen atom from the other complex unit, and these nitrogen-coordinated geminal Cu(I) atoms of one unit then bind directly to the similarly nitrogen coordinated geminal Cu(I) of the other ligand unit by means of a direct Cu−Cu linkage. This connection forms the "bottom" of the cluster. The ligand does not form a complete "pincer" structure about an individual metal. Two additional CuX units, each coordinated to the second, available, nitrogen atom of the ligand, are incorporated by binding directly, via a Cu(I)−Cu(I) bond, to the carbon substituted geminal Cu(I) atom, and the appended X substituent (Me or halide) on this inserted unit then coordinates to another geminal Cu(I) atom to form Cu−X−Cu bridges spanning the open face of the initial framework, thereby assembling a capped boat-shaped Cu_6 cluster (Figure 1). Each PCP pincer ligand is thus bound to two "bottom" copper atoms (on different units) via carbon and nitrogen atoms, and these copper atoms bind to each other directly to form a C−Cu−Cu−C edge. Each of the component ($NPCCu_2$) units is relatively flat. The ligand carbon bridged group of four Cu(I) atoms thus forms the body of a boat with the other two Cu(I) atoms of the CuX units appearing as the "stem" and "stern" (Figures 1 and 2) of the boat. As shown in Figure 1, the pincer ligands surrounding the $Cu(I)_6$ core structure of three halide complexes (**2**−**4**) have a similar configuration. Although similarly constructed, the methyl-bridged complex **1** is different in that the conformation has a mirror symmetry relative to that of **2**−**4**.

Within the unit cell of the chloride-bridged complex **2**, there are two different cluster molecules showing slightly different bond distances and angles. These are labeled $Cu_A(I)_6$ and $Cu_B(I)_6$. In **3** and **4** there is only one cluster arrangement. When comparing the three halide clusters, we see that the Cu−X−Cu bond angles irregularly change through the series Cl to I (average Cu−Cl−Cu = 77.57°, Cu−Br−Cu = 72.83° and Cu−I−Cu = 65.20°) so that the length trend provides a medium value for the Cl case (2.704 Å; **2**), the longest value for the Br case (2.718 Å; **3**), and the shortest value for the I case (2.656 Å; **4**). The Cu−C−Cu bond angles in both the bridged methyl complex **1** and the bromide complex **3** are similar (Cu−C−Cu = 73.00°); however, the shorter Cu−C (2.018(3) Å) bond distances in **1** compared to those of the Cu−Br complex **3** (2.2893(6) Å) lead to the result that the shortest Cu−Cu bond distance (2.403(3) Å) is found in structure **1**. It has also been found throughout that the bond distances between the bridging atom (C, Cl, Br, and I) and the two Cu(I) atoms are not equal; one is always slightly longer than the other. The average differences are 0.067 (**1**), 0.021 (**2**), 0.048 (**3**) and 0.020 Å (**4**), with the largest difference occurring in **1**. Close examination of the structure of **1** shows that there are dissimilar, close approach bond distances between the methyl protons and nearby copper(I) atoms; Cu(5)−H(3A) = 1.957 Å and Cu(6)−H(4A) = 1.850 Å, which indicates the presence of additional agnostic bonding interactions which may contribute to the differences between the carbon−copper bonds (see the Supporting Information).

The intramolecular Cu···Cu separations fall in the range 2.4000(4)−2.9458(5) Å, which are shorter than or close to the sum of the van der Waals radii of Cu(I) centers. Separations increase in the following order: **1** (average separations 2.6493(4) Å), **4** (average 2.6956(8) Å), **3** (average 2.7251(7) Å), and **2** (average 2.7342(6) for molecule **A** and average 2.7250(6) Å for molecule **B**). These average Cu···Cu separations are all slightly longer than that previously reported for the octahedron of copper atoms in $Cu_6Fe_4(CO)_{16}^{2-}$ anions in the complex $[(diphos)_2Cu]_2Cu_6Fe_4(CO)_{16}$ (average 2.616 Å),[8] but all are substantially shorter than those in the complex

(8) Doyle, D.; Eriksen, K. A.; Van Engen, D. *J. Am. Chem. Soc.* **1985**, *107*, 7914–7920.

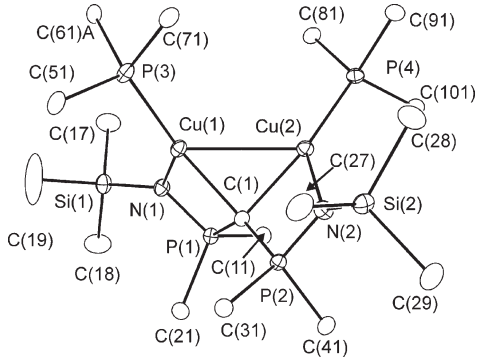

Figure 3. Perspective view of complex **6** showing the atom-labeling scheme. Only the ipso carbons of the phenyl groups are shown. Hydrogen atoms are omitted. Non-hydrogen atoms are represented by Gaussian ellipsoids at the 20% probability level. Bond lengths and angles are given in Table 2.

$[Cu_6(6\text{-mpyt})_6]$ (6-mpyt = 6-methyl-2-pyridinethiolato; 2.831(1)−3.326(2) Å).[1e] The Cu−Cu separations here are very similar to those in the Cu_6 cluster assembly, wherein a tridentate nitrogen ligand (*N*,*N*′,*N*″-trimethyl-1,3,5-triazacyclohexane) is supported with a bridging Cl.[9] The two C−Cu bond distances to the PCP-bridged carbon connecting two copper atoms in clusters **1**−**4** are all different, and of note is that one is slightly shorter than the other. Similarly, the P−N and P−C bond distances within the chelate ligand are slightly different, which creates the nonidentical P environments consistent with the observed AB ^{31}P NMR spectra.

The solid-state structure of the bimetallic complex **6** was investigated by means of single-crystal X-ray diffraction with the result shown in Figure 3. Selected bond lengths and angles and data collection parameters are given in Tables 2 and 3. The core structure of **6** (Figure 3) shows two copper atoms bridged by a pincer carbon structure. Each copper center is thus coordinated to three different donor atoms (the pincer bridging carbon, a N, and a P) and bound to the other copper (the Cu(1)−Cu(2) distance is 2.7217(6) Å), making a four-coordinated metal center with a distorted-tetrahedral geometry. Two heterocyclic four-membered rings (Cu(1)-C(1)P(1)N(1) and Cu(2)C(1)P(2)N(2)) are connected through the two side borders of the three-membered ring (Cu(1)-Cu(2)C(1)), and one points up and one points down relative to the plane of the three-membered ring, forming a chair conformation. The Cu−N (Cu(1)−N(1) = 2.142(3), Cu(2)−N(2) = 2.126(3) Å) and Cu−P lengths (Cu(1)−P(3) = 2.1608(9), Cu(2)−P(4) = 2.1582(9) Å) are in the expected range (e.g., Cu−N = 2.058(2)−2.074(2) Å and Cu−P = 2.1756(7) Å in $[\{CH(PPh_2N{=}SiMe_3)_2\}CuPPh_3]$[7] and Cu−N = 2.116(7) and 2.121(6) Å and Cu−P = 2.244(2) Å in *cis*-$[Cu_2(\mu\text{-CN})(Phen)(PPh_3)_2]_2[C(CN)_3]\cdot BF_4\cdot 2CH_3CN$[10]). The Cu−C bond distances (Cu(1)−C(1) = 2.031(3) Å and Cu(2)−C(1) = 2.045(3) Å) in **6** are remarkably longer than that in the dicoordinate copper structure (e.g., 1.916(2) Å in $[Cy_3PCuCH_3]$)[11] and even longer than these in the tricoordinate structures (e.g., Cu−C = 1.921(3) Å in [Cu(CN)(dppm)][12] and Cu−C = 1.931(5) Å in $[Cu(CN)(PCy_3)]_6$[13]). However, the distances in **6** are compatible with four-coordinate copper for tetrahedral structures (e.g., Cu−C = 2.01(2) Å of [Cu(en=P_2)-(*t*-BuNC)](ClO_4) (en=P_2 = *N*,*N*′-bis[*o*-(diphenylphosphino)-benzylidene]ethylenediamine)[14a] and Cu−C = 1.988(2) Å of $[Cu(CN)(PPh_3)_2]_6$[14b]), which indicates that structure **6** has a four-coordinate copper center. The Cu−Cu distance in **6** (Cu(1)−Cu(2) = 2.7217(6) Å) is compatible with the observed bond distances in **2**−**4** and also shows a weakly bonding interaction.

As we mentioned above, an unexpected single-copper complex of the parent (iminophosphorano)methane ligand, **7**, was detected as a minor component during the preparation of cluster **4**. Green crystals were obtained, and its structure is illustrated in Figure 4 (selected bond lengths and angles and data collection parameters are given in Tables 2 and 3). The PCP bridging carbon is doubly protonated; thus, here the H_2L ligand behaves simply as a bidentate ligand, binding to copper through two nitrogen atoms forming, along with the bound I, a three-coordinate copper center. The Cu−N and Cu−I bond distances (Cu−N(N′) = 2.0480(19) Å, Cu−I = 2.5071(5) Å) in **7** are remarkably shorter than those in the four-coordinate structure[15] but are compatible with those of other reported three-coordinate copper centers of the type (CuN_2I).[16] The six-membered ring (Cu−N−P−CH_2−P′−N′) is in a chair configuration, and the four atoms of N, P, P′, and N′ are located exactly in a plane. The mirror plane is preserved through the three-atom sets, the methylene C, Cu, and I.

All four isolated cluster complexes **1**−**4** are quite stable in the solid state under an inert atmosphere at room temperature, and they seem to be reasonably stable in the open atmosphere. They can be kept for a few weeks in the air without any observable color or weight change. In solution, all complexes are quite stable in the glovebox atmosphere, but upon exposure to air the complexes in solution are slowly oxidized to materials with a blue color. The electrospray mass spectra shows a molecular mass peak of all clusters with the complete isotopic pattern for six copper atoms at 1524.0 (**1**), 1565.9 (**2**), 1653.8 (**3**), and 1747.8 amu (**4**) respectively (see the Supporting Information). The spectral pattern is identical with that simulated from the molecular formula. Thus, these clusters are stable in the gas phase in the spectrometer environment. Thermogravimetric analysis (TGA) indicated a decomposition temperature range for clusters **2**−**4** between 200 and 500 °C, whereas **1** the decomposition range is 300−500 °C. Overall the copper clusters are quite thermally stable, with complex **1** being the least stable member.

Some preliminary reactivity of the complex $[Cu_6L_2Cl_2]$ (**2**; L = $C(Ph_2P{=}NSiMe_3)_2^{2-}$) has been investigated. Quantitative addition of 2 mol of $LiCH_3$ to a THF solution of **2**

(9) Köhn, R. D.; Pan, Z.; Mahon, M. F.; Kociok-Köhn, G. *Chem. Commun.* **2003**, 1272–1273.
(10) Kamte, M. F.; Baumeister, U.; Schäfer, W. *Z. Anorg. Allg. Chem.* **2003**, *629*, 1919–1924.
(11) Schaper, F.; Foley, S. R.; Jordan, R. F. *J. Am. Chem. Soc.* **2004**, *126*, 2115–2124.
(12) Di Nicola, C.; Effendy; Pettinari, C.; Skelton, B. W.; Somers, N.; White, A. H. *Inorg. Chim. Acta* **2006**, *359*, 53–63.
(13) Lin, Y.-Y.; Cai, S.-W.; Che, C.-M.; Fu, W.-F.; Zhou, Z.-Y.; Zhu, N-Y *Inorg. Chem.* **2005**, *44*, 1511–1524.
(14) (a) Jeffery, J. C.; Rauchfuss, T. B.; Tucker, P. A. *Inorg. Chem.* **1980**, *19*, 3306–3315. (b) Zhao, Y.; Hong, M.; Su, W.; Cao, R.; Zhou, Z. *Dalton Trans.* **2000**, 1685–1686.
(15) Niu, Y.-Y.; Zhang, N.; Hou, H.-W.; Zhu, Y.; Tang, M.-S.; Ng, S.-W. *J. Mol. Struct.* **2007**, *827*, 195–200.
(16) (a) Muhle, J.; Sheldrick, W. S. *Z. Anorg. Allg. Chem.* **2003**, *629*, 2097–2102. (b) Healy, P. C.; Pakawatchai, C.; White, A. H. *J. Chem. Soc., Dalton Trans.* **1983**, 1917–1927. (c) Walsdorff, C.; Park, S.; Kim, J.; Heo, J.; Park, K.; Oh, J.; Kim, K. *J. Chem. Soc., Dalton Trans.* **1999**, 923–930. (d) Toth, A.; Floriani, C.; Chiesi-Villa, A.; Guastini, C. *Inorg. Chem.* **1987**, *26*, 3897–3902. (e) Dyason, J. C.; Engdhardt, L. M.; Healy, P. C.; Kildea, J. D.; White, A. H. *Aust. J. Chem.* **1988**, *41*, 335–340. (f) Pohl, S.; Harmjanz, M.; Schneider, J.; Saak, W.; Henkel, G. *Dalton Trans.* **2000**, 3473–3479. (g) Zhao, S.-B.; Wang, R.-Y.; Wang, S.-N. *Inorg. Chem.* **2006**, *45*, 5830–5840. (h) Domaservitch, K. V.; Solntsev, P. V.; Sieler, J. *Zh. Strukt. Khim.* (*J. Struct. Chem.*) **2005**, *46* (suppl), S145–S151.

Table 2. Selected Bond Lengths (Å) and Angles (deg) for Compounds 1−4, 6, and 7

Compound **1**

Cu(4)−Cu(6)	2.4000(4)	Cu(2)−Cu(3)	2.5649(4)
Cu(1)−Cu(6)	2.6128(4)	Cu(2)−C(1)	1.961(2)
Cu(1)−Cu(5)	2.4047(4)	Cu(6)−C(1)	1.993(2)
Cu(4)−Cu(5)	2.6512(4)	Cu(3)−C(2)	1.953(2)
Cu(4)−Cu(3)	2.7496(4)	Cu(5)−C(2)	1.992(2)
Cu(2)−Cu(6)	2.7732(4)	Cu(1)−C(3)	1.979(2)
Cu(1)−Cu(2)	2.7546(4)	Cu(5)−C(3)	2.057(3)
Cu(3)−Cu(5)	2.7785(4)		
Cu(2)−Cu(3)−Cu(4)	104.647(12)	Cu(2)−Cu(5)−Cu(3)	56.330(10)
Cu(2)−Cu(3)−Cu(5)	59.307(10)	P(1)−C(1)−P(2)	129.63(12)
Cu(1)−Cu(2)−Cu(3)	105.540(12)	P(3)−C(2)−P(4)	129.51(12)
Cu(3)−Cu(2)−Cu(6)	60.733(10)	Cu(4)−C(4)−Cu(6)	72.89(8)
Cu(5)−Cu(1)−Cu(6)	66.244(12)	N(3)−Cu(4)−C(4)	158.11(9)
Cu(1)−Cu(5)−Cu(4)	104.475(14)	N(2)−Cu(3)−C(2)	174.12(9)
Cu(1)−Cu(6)−Cu(4)	105.788(14)	C(1)−Cu(6)−C(4)	159.50(9)

Compound **2**

Cu(4B)−Cu(6B)	2.6624(6)	Cu(2B)−Cu(3B)	2.5982(5)
Cu(4B)−Cu(5B)	2.6510(6)	Cu(2B)−C(1B)	1.954(3)
Cu(1B)−Cu(5B)	2.7429(6)	Cu(6B)−C(1B)	1.966(3)
Cu(1B)−Cu(6B)	2.6264(6)	Cu(3B)−C(2B)	1.945(3)
Cu(2B)−Cu(6B)	2.7301(5)	Cu(5B)−C(2B)	1.967(3)
Cu(3B)−Cu(4B)	2.7688(5)	Cu(5B)−C(2B)	1.967(3)
Cu(3B)−Cu(5B)	2.7397(5)	Cu(1B)−Cl(1B)	2.1447(10)
Cu(1B)−Cu(2B)	2.8317(6)	Cu(5B)−Cl(1B)	2.1659(10)
Cu(2B)−Cu(3B)−Cu(4B)	107.619(18)	Cu(2B)−Cu(5B)−Cu(3B)	56.390(13)
Cu(2B)−Cu(3B)−Cu(5B)	62.188(14)	P(1B)−C(1B)−P(2B)	128.91(18)
Cu(1B)−Cu(2B)−Cu(3B)	106.360(17)	P(3B)−C(2B)−P(4B)	129.81(18)
Cu(3B)−Cu(2B)−Cu(6B)	60.980(14)	Cu(1B)−Cl(1B)−Cu(5B)	79.04(3)
Cu(5B)−Cu(1B)−Cu(6B)	64.933(16)	Cl(1B)−Cu(1B)−N(1B)	164.54(8)
Cu(1B)−Cu(5B)−Cu(4B)	102.173(17)	N(2B)−Cu(3B)−C(2B)	174.55(12)
Cu(1B)−Cu(6B)−Cu(4B)	106.452(19)	Cl(1B)−Cu(5B)−C(2B)	163.19(9)

Compound **3**

Cu(4)−Cu(6)	2.7109(7)	Cu(2)−Cu(3)	2.5853(6)
Cu(4)−Cu(5)	2.6472(7)	Cu(2)−C(1)	1.944(4)
Cu(1)−Cu(5)	2.7254(7)	Cu(6)−C(1)	1.981(4)
Cu(1)−Cu(6)	2.6288(7)	Cu(3)−C(2)	1.948(4)
Cu(2)−Cu(6)	2.7629(6)	Cu(5)−C(2)	1.974(4)
Cu(3)−Cu(4)	2.7894(7)	Br(1)−Cu(5)	2.3077(6)
Cu(3)−Cu(5)	2.7300(6)	Br(1)−Cu(1)	2.2658(6)
Cu(1)−Cu(2)	2.8031(7)		
Cu(2)−Cu(3)−Cu(4)	108.64(2)	Cu(2)−Cu(5)−Cu(3)	56.396(16)
Cu(2)−Cu(3)−Cu(5)	62.025(17)	P(1)−C(1)−P(2)	128.0(2)
Cu(1)−Cu(2)−Cu(3)	107.01(2)	P(3)−C(2)−P(4)	128.0(2)
Cu(3)−Cu(2)−Cu(6)	61.065(17)	Cu(4)−Br(2)−Cu(6)	72.51(2)
Cu(5)−Cu(1)−Cu(6)	64.436(18)	N(3)−Cu(4)−Br(2)	161.56(10)
Cu(1)−Cu(5)−Cu(4)	106.39(2)	N(2)−Cu(3)−C(2)	174.73(14)
Cu(1)−Cu(6)−Cu(4)	107.34(2)	C(1)−Cu(6)−Br(2)	159.62(11)

Compound **4**

Cu(4)−Cu(6)	2.6480(7)	Cu(2)−Cu(3)	2.6052(6)
Cu(4)−Cu(5)	2.6391(9)	Cu(2)−C(10)	1.942(4)
Cu(1)−Cu(5)	2.6630(8)	Cu(6)−C(10)	1.989(4)
Cu(1)−Cu(6)	2.6308(8)	Cu(3)−C(20)	1.944(4)
Cu(2)−Cu(6)	2.7373(7)	Cu(5)−C(20)	1.983(4)
Cu(3)−Cu(4)	2.6805(7)	I(1)−Cu(5)	2.4716(6)
Cu(3)−Cu(5)	2.7583(7)	I(1)−Cu(1)	2.4531(7)
Cu(1)−Cu(2)	2.6983(7)		
Cu(2)−Cu(3)−Cu(4)	106.56(2)	Cu(2)−Cu(5)−Cu(3)	57.328(17)
Cu(2)−Cu(3)−Cu(5)	59.639(18)	P(1)−C(10)−P(2)	130.1(2)
Cu(1)−Cu(2)−Cu(3)	107.29(2)	P(3)−C(20)−P(4)	130.6(2)
Cu(3)−Cu(2)−Cu(6)	60.278(18)	Cu(4)−I(1)−Cu(6)	64.933(19)

Table 2. Continued

Cu(5)−Cu(1)−Cu(6)	67.26(2)	I(2)−Cu(6)−C(10)	159.13(11)
Cu(1)−Cu(5)−Cu(4)	104.01(3)	N(2)−Cu(3)−C(20)	175.22(17)
Cu(1)−Cu(6)−Cu(4)	104.67(3)	I(2)−Cu(4)−N(3)	155.58(11)

Compound **6**

Cu(1)−Cu(2)	2.7217(6)	Cu(2)−P(4)	2.1582(9)
Cu(1)−P(3)	2.1608(9)	Cu(2)−N(2)	2.126(3)
Cu(1)−N(1)	2.142(3)	Cu(2)−C(1)	2.045(3)
Cu(1)−C(1)	2.031(3)		
Cu(2)−Cu(1)−P(3)	116.60(3)	C(1)−Cu(2)−N(2)	77.81(11)
Cu(1)−Cu(2)−P(4)	119.40(3)	C(1)−Cu(1)−Cu(2)	48.32(8)
C(1)−Cu(1)−P(3)	152.45(9)	N(1)−Cu(1)−P(3)	128.46(7)
C(1)−Cu(2)−P(4)	145.90(8)	P(1)−C(1)−P(2)	134.75(18)

Compound **7**

Cu−I	2.5071(5)	P−N	1.5694(19)
Cu−N	2.0480(19)	P−C(10)	1.8249(16)
Cu−N′	2.0480(19)	P′−C(10)	1.8249(16)
I−Cu−N	127.64(5)	N−P−C(10)	111.78(12)
I−Cu−N′	127.64(5)	P′−C(10)−P	118.36(16)
N−Cu−N′	104.57(11)		

resulted in an immediate color change from bright yellow to green. The ^{31}P NMR measurement of the resultant solution showed clearly that the product was complex **1**, which was subsequently isolated from the solution and the identity confirmed. A solution containing the isolated complex **2** was treated with 2 mol of NaO^{t}Bu in THF in slight excess. Monitoring the reaction by ^{31}P NMR showed that the reaction proceeded very slowly, taking several days at room temperature. Throughout the reaction period we observed the initial buildup of 12 peaks in 3 pairs of AB coupling patterns, which could be assigned to the cluster species $[Cu_6L_2Cl_2]$ (the starting material), $[Cu_6L_2(O^tBu)Cl]$ (an intermediate), and $[Cu_6L_2(O^tBu)_2]$ (**5**) (the final product). Eventually, the ^{31}P NMR spectrum showed only one final set of four peaks with an AB coupling pattern (Scheme 3), which can be assigned to **5**. It is interesting that these new species can be generated by simple substitution reactions without disrupting the six-copper core cluster structure. The new cluster **5** may show some novel reactivity or catalytic properties and is presently under study.

Absorption spectra of **1**−**4** in solution are shown in Figure 5a. All compounds display strong absorption peaks in the UV (∼300 nm, $\varepsilon \approx 10^4$ L cm^{-1} M^{-1}) and near-visible regions (∼425 nm, $\varepsilon \approx 5 \times 10^3$ L cm^{-1} M^{-1}), in addition to weaker bands or shoulders in between. Spectral data are summarized in Table 4. The spectral patterns for **2**−**4** were very similar to each other, with the shorter wavelength absorption appearing as peaks at 299, 302, and 301 nm and longer wavelength absorption appearing as peaks at 409, 413, and 423 nm in the case of **2**−**4**, respectively. Much weaker shoulders were present at 360 and 362 nm for **2** and **3**, and an even weaker shoulder appears at 364 nm in the case of **4**. Complex **1** showed, in contrast, only two peaks at 294 and 427 nm. Following the literature,[17] we assign the strong peak in the UV region to metal-centered metal−metal 3d → 4p transitions, while the peak in the near-visible region is most likely due to ligand to metal charge transfer (LMCT) and metal-centered d → s transitions. The strong peak in the UV region nicely matches the energy gap between the HOMO and LUMO, as shown by the DFT calculations (the calculated HOMO and LUMO energy gaps are 300, 282, 290, and 330 nm for **1**−**4**, respectively). The DFT molecular orbital coefficients show that the HOMO component is dominated by copper d orbitals and the LUMO is mainly composed of copper p orbitals (see the Supporting Information), thereby providing support for the absorption band assignments to 3d → 4p transitions. The weak shoulders on the three halide complexes (**2**−**4**) could be due to either halide to metal charge transfer (XMCT) or halide to ligand charge transfer (XLCT) because complex **1**, which is halide-free, does not show this shoulder. Additional information from the spectrum of **7** (see below and Figure 5a) supports the former interpretation (XMCT), as the latter (XLCT) is unlikely in this simple chelate. Similar absorption bands were previously observed in the dimeric copper complex $[Cu_2(dcpm)_2]X_2$[1f] (dcpm = bis(dicyclohexylphosphanyl)-methane) and the hexanuclear octahedral copper complex $Cu_6(mtc)$[18] (mtc$^-$ = di-*n*-propylmonothiocarbamate), where assignments were similar.[17] The absorption spectra of Cu(I) halides have also been attributed to mixed d → s/LMCT transitions.

The Cu−Cu bond distances shown in the molecular structures **1**−**4** decrease in the order **1**, **2**, **4**, and **3**, which is in the same order as shown by the UV absorption peak energies (294 (**1**), 299 (**2**), 301 (**4**), and 302 nm (**3**)), suggesting a correlation between bond lengths and absorption peak energy; thus, complexes **2**−**4** show a halide effect on the transition energies of the absorption peaks (Figure 5a).

Similar to the case for **1**, the monocopper iodide complex $[CuI(H_2L)]$ (**7**) displays two strong peaks at 296 and 365 nm, respectively (Figure 5a). Because there is only one copper atom present in this structure, the absorption peak is shifted to a high-energy wavelength compared to those for the six-copper clusters. We note that the second peak at 365 nm in **7** is very close to the shoulder peaks which appear in the three halide clusters. As halide to metal charge transfer (XMCT) is the most likely process for **7**, we suggest that the absorption spectrum of **7** provides reasonable evidence for halide to metal charge transfer (XMCT) in the six-copper clusters (**1**−**4**).

(17) Ford, P. C.; Vogler, A. *Acc. Chem. Res.* **1993**, *26*, 220–226.

(18) Sabin, F.; Ryu, C. K.; Ford, P. C.; Vogler, A. *Inorg. Chem.* **1992**, *31*, 1941–1945.

Table 3. Crystal Data and Structure Refinement Details for 1−4, 6, and 7

	$C_{72}H_{98}Cu_6N_4O_2P_4Si_4$ (**1**)	$C_{69}H_{93.5}Cl_2Cu_6N_4O_{1.75}P_4Si_4$ (**2**)	$C_{62}H_{76}Br_2Cu_6N_4P_4Si_4$ (**3**)	$C_{64}H_{81}Cu_6I_2N_4O_{0.5}P_4Si_4$ (**4**)	$C_{74}H_{76}Cu_2N_2P_4Si_2$ (**6**)	$C_{35}H_{50}CuIN_2OP_2Si_2$ (**7**)
fw	1669.02	1695.36	1654.57	1785.61	1300.51	823.33
cryst syst	orthorhombic	triclinic	orthorhombic	monoclinic	triclinic	monoclinic
cryst dimens (mm)	0.48 × 0.41 × 0.27	0.32 × 0.30 × 0.20	0.25 × 0.24 × 0.14	0.33 × 0.31 × 0.25	0.38 × 0.31 × 0.29	0.37 × 0.29 × 0.23
space group	*Pbca* (No. 61)	$P\bar{1}$ (No. 2)	$P2_12_12_1$ (No. 19)	$P2_1/n$ ($P2_1/c$, No. 14)	$P\bar{1}$ (No. 2)	$P2_1/m$ (No. 11)
unit cell dimens						
a (Å)	22.8100(15)	14.4174(5)	16.0037(9)	14.6629(8)	13.228(2)	9.4818(4)
b (Å)	24.5879(16)	21.7660(7)	19.4167(11)	23.1444(12)	13.701(2)	18.8992(7)
c (Å)	27.1406(18)	25.9932(8)	22.5945(12)	21.4145(11)	20.800(3)	11.7168(4)
α (deg)		100.5122(4)			107.4218(18)	
β (deg)		98.6051(4)		99.6880(10)	90.3296(18)	109.6397(4)
γ (deg)		97.5673(4)			96.2947(19)	
V (Å^3)	15221.8(17)	7792.9(4)	7021.0(7)	7163.7(7)	3572.2(9)	1977.49(13)
Z	8	4	4	4	2	2
calcd density (g cm^{-3})	1.457	1.455	1.565	1.656	1.209	1.383
temp (K)	173.2(1)	173.2(1)	173.2(1)	173.2(1)	173.2(1)	193.2(1)
μ(Mo Kα) (mm^{-1})	1.839	1.863	3.122	2.809	0.759	1.502
θ range for data collecn (deg)	2.24−26.18	2.21−25.99	2.21−18.49	2.50−27.36	2.32−26.31	2.28−27.58
index ranges	$-28 \le h \le 28$	$-18 \le h \le 18$	$-20 \le h \le 20$	$-19 \le h \le 19$	$-16 \le h \le 16$	$-12 \le h \le 12$
	$-30 \le k \le 30$	$-27 \le k \le 27$	$-25 \le k \le 25$	$-30 \le k \le 29$	$-17 \le k \le 17$	$-24 \le k \le 24$
	$-33 \le l \le 33$	$-32 \le l \le 32$	$-29 \le l \le 29$	$-27 \le l \le 27$	$-26 \le l \le 25$	$-15 \le l \le 12$
no. of rflns collected	15 594	32 339	16 121	16 410	14 591	4678
no. of indep rflns	12 598	23 223	13 648	13 756	12 046	4232
no. of data/restraints/params	15 594/0/829	32 339/20/1657	16 121/0/739	16 410/7/758	14 591/4/787	4678/0/211
goodness of fit on F^2	1.016	1.010	1.024	1.025	1.082	1.056
final R indices ($I \ge 2\sigma(I)$)						
R1	0.0279	0.0366	0.0348	0.0485	0.0478	0.0335
wR2	0.0709	0.0997	0.0796	0.1331	0.1588	0.0930
largest diff peak and hole (e/Å^3)	0.640 and −0.471	0.726 and −0.553	1.966 and −0.681	3.480 and −2.196	1.144 and −0.655	1.506 and −1.083

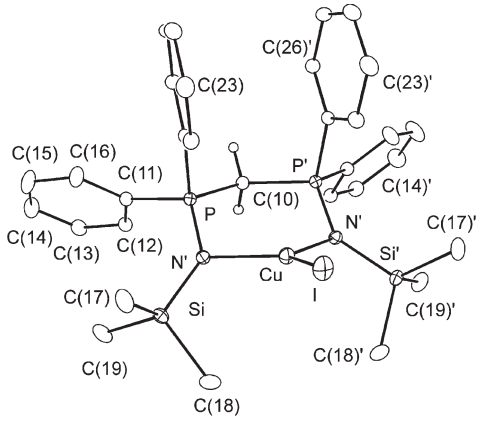

Figure 4. Perspective view of the complex [CuI{CH_2(PPh_2=$NSiMe_3$)$_2$}] (**7**) showing the atom-labeling scheme. Primed atoms are related to unprimed ones by the mirror plane located at x, $^1/_4$, z. Non-hydrogen atoms are represented by Gaussian ellipsoids at the 20% probability level. Hydrogen atoms are shown with arbitrarily small thermal parameters for the methylene group and are not shown for the methyl and phenyl groups. Bond lengths and angles are given in Table 2.

Scheme 3. Reaction of 2 with MeLi To Form 1 and with NaO^{t}Bu To Form 5

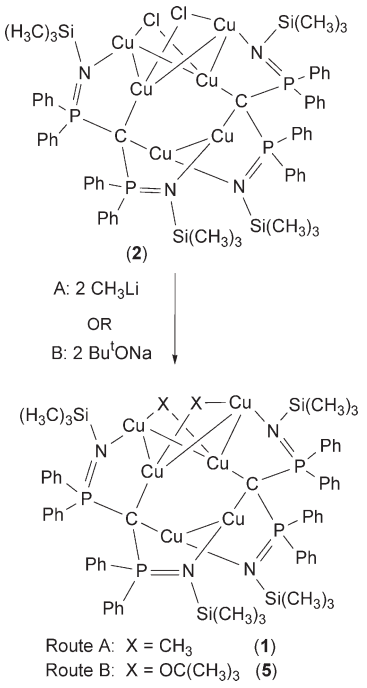

In the solid state, the hexanuclear copper complexes (**1**−**4**) show intense photoluminescence spectra (Figure 5b). At ambient temperatures one intense low-energy emission at λ_{max}^{em} 579 nm (or 17 271 cm^{-1}) was detected for complex **1** and **2**−**4** show two emission bands; respectively intense low energy (LE) bands at 631 (15 848 cm^{-1}), 655 (15 267 cm^{-1}), and 659 nm (15 175 cm^{-1}) and much weaker, higher energy (HE) bands at 528 (18 940 cm^{-1}), 566 (17 668 cm^{-1}), and 570 nm (17 544 cm^{-1}). The bright LE emission band of **1** can

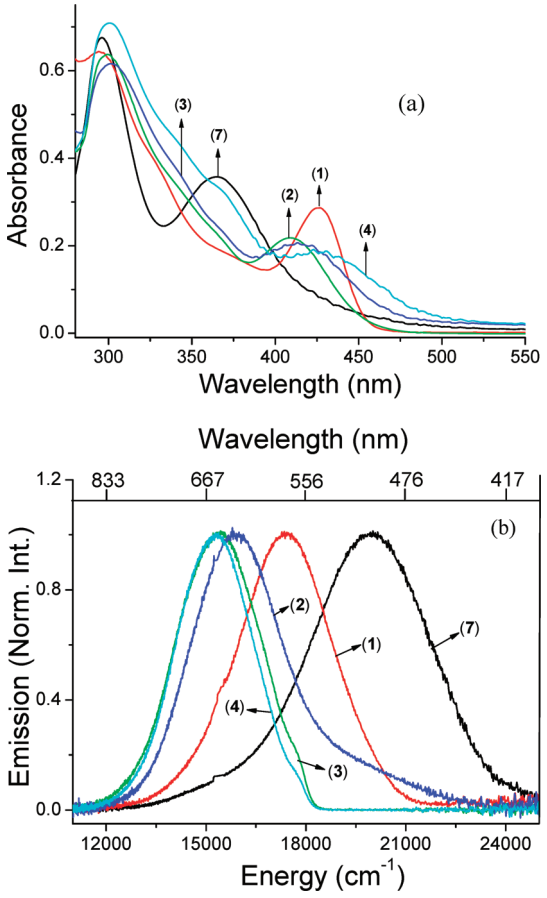

Figure 5. (a) UV−vis solution absorption spectra of **1**−**4** and **7** and (b) solid-state emission spectra of the same complexes excited (ex) with 325 nm radiation provided by a He−Cd laser source. Note that the absorption and emission maxima of **7** are substantially different from those of **1**−**4** because of a difference in molecular structure.

be assigned to the Cu_6 cluster d ← s transition.[18,19] Relative to **1**, the emission bands of **2**−**4** show a red shift trend and the presence of weaker HE bands suggests some halogen participation in the emission spectra. This emissive state has mixed d−s/XMCT character delocalized over the Cu_6X_2 core with roughly equal contributions from each component.[17,20] The mixed d−s/XLCT excited state accounts for the HE emission band in each system.[19] The very large Stokes shift for the LE emission band of the Cu_6X_2 core clusters is consistent with this assignment for the transitions. These assignments are also consistent with early studies of the $Cu_4I_4(Py)_2$ (Py = pyridine) core system.[17−20] There is a clear trend connecting absorption wavelength and emission energies which follows the nature of the bridging substituents, suggesting that substitution of the capping ligand on the cluster could be used to control the values of the optical properties.

The monocopper iodide complex **7** also shows a symmetric photoluminescence peak at λ_{max}^{em} 496 nm (or 20 160 cm^{-1}) similar to that of **1** without any additional shoulder or weak bands; thus, these features likely arise from within the cluster unit.

The bright emission colors of the four copper clusters **1**−**4** can be seen both in the solid state and in solution (with colors

(19) Kyle, K. R.; Ryu, C. K.; DiBenedetto, J. A.; Ford, P. C. *J. Am. Chem. Soc.* **1991**, *113*, 2954–2965.

(20) Vitale, M.; Palke, W. E.; Ford, P. C. *J. Phys. Chem.* **1992**, *96*, 8329–8336.

Table 4. Summary of Absorption, Emission, and Excitation Spectral Data for Compounds 1−4 and 7[a]

compd	absorbance	excitation/toluene	emission/toluene	emission/solid	QY
1	427 (9.9×10^3), 294 (2.1×10^4)	326, 420	605, 701 (sh)	579 (b)	0.75
2	409 (7.9×10^3), 299 (2.3×10^4)	342, 421	633, 703 (sh)	631 (b), 528 (s)	0.71
3	419 (6.5×10^3), 302 (2.0×10^4)			655 (b), 566 (s)	
4	423 (9.9×10^3), 301 (3.8×10^4)	365, 451	648, 714 (sh)	659 (b), 570 (s)	0.62
7	365 (6.8×10^3), 296 (1.3×10^4)			496 (b)	

[a] All wavelengths are given in nm and extinction coefficients (in parentheses) in L cm^{-1} M^{-1}. Legend: sh = shoulder, b = big, s = small.

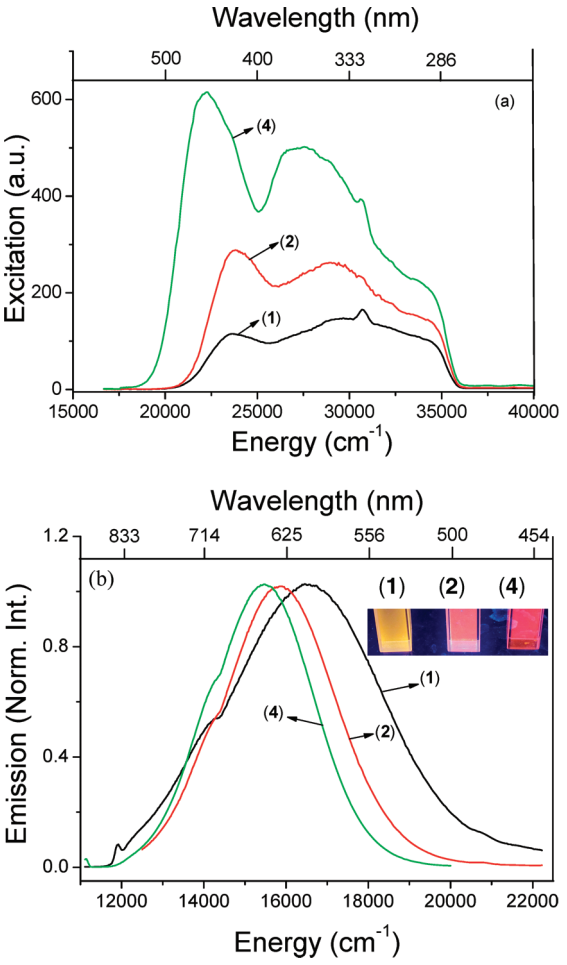

Figure 6. (a) Excitation spectra of **1**, **2**, and **4** in toluene. Note that maximum excitation for **1** and **2** occurs at 420 nm and that for **4** at 450 nm. (b) Emission spectra for complexes obtained by excitation (ex) at the maximum indicated by the excitation spectra: 420 nm in the case of **1** and **2** and 450 nm for **4**. The inset shows the color of emission under broad-band UV light for these three complexes.

ranging from yellow to orange to red). The photoluminescent spectra of the solid materials are shown in Figure 5b, and data are given in Table 4. The emission peaks shift toward lower energy through the series **1**, **2**, and **4**. The emission peaks of **3** and **4** are very close to each other. In solution, the emission and excitation spectra of compounds **1**, **2**, and **4** are very similar, as indicated in Figure 6 (with numerical data given in Table 4). The excitations of these three compounds in solution show very similar spectral patterns, with two large excitation peaks (Figure 6b and Table 4). In solution again there is a shift of the excitation peaks to lower energy through the series **1** to **2** and **4**. The qualitative relationships between emission and absorbance energies is illustrated in Figure 7.

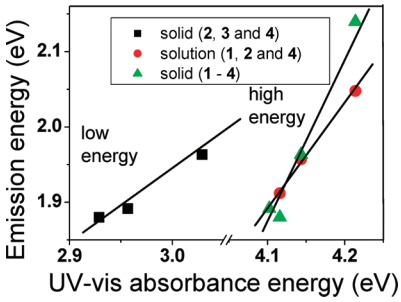

Figure 7. Relationship between emission and absorbance energies of the hexacopper clusters **1**−**4**. The connecting lines are not linear fits but rather association connections.

The intensities of the solution emission spectra excited by two different energies, 325 or 420 nm, 342 or 420 nm, and 365 or 450 nm for compounds **1**, **2**, and **4**, respectively (corresponding to the two main excitation peaks observed in all solution cases, as shown in Figure 6a with data given in Table 4) were compared in order to evaluate which value of excitation energy yielded the more intense emission. In all cases the lower energy excitation (420 nm in the case of **1** and **2** and 450 nm in the case of **4**) yielded the highest intensity emission compared to its higher energy excitation at 325, 342, and 365 nm. In each case the same emission peak shape (or spectral pattern) was detected (Figure 6b) for each compound regardless of the excitation energy. The solution emission spectra are also very similar to the spectra recorded for the solids, except for slight differences in peak position probably caused by solvent effects.

That different excitation energies, for either the solids or the solutions, yield the same emission spectrum indicates that the emission energy gap is a constant defined by the molecular cluster. The quantum yields of these compounds were determined in highly dilute concentrations in toluene through comparison to a similarly dilute solution of a Rhodamine 590 standard using the same measurement conditions (Table 4). The measured quantum yields were 0.75, 0.71, and 0.62, respectively, for **1**, **2**, and **4**, which are higher than those reported for the carbon-bridged tetraatomic copper cluster (QY = 0.42)[2s] but are lower than the highest value reported for a mixed copper−gold cluster (QY = 0.92).[2t] Overall, these copper clusters are highly photoefficient compounds. Moreover, their quantum yields are comparable through the hexaatomic series, indicating that the emission is generated by the boat-shaped hexaatomic copper cluster core.

Additional insight into the character of the transitions was provided by a TD-DFT calculation on the core structure of cluster **2**, a representative example of the six-copper cluster series. The results showed two allowed singlet excited state transitions: ES_1 ($=S_0 \rightarrow S_1$) at 344.81 nm ($f = 0.0116$) with an energy gap of 3.5957 eV and ES_2 ($=S_0 \rightarrow S_2$) at 321.37 nm ($f = 0.0286$) with an energy gap of 3.8580 eV. One forbidden

transition at 331.85 nm ($f = 0.0000$) with an energy gap of 3.7362 eV was also calculated. ES_1 is derived from the three molecular orbital combinations HOMO-2 → LUMO (coeff = 0.1806), HOMO → LUMO (coeff = 0.6550), and HOMO → LUMO+1 (coeff = −0.1115), while ES_2 involves the three combinations HOMO-2 → LUMO (coeff = 0.6388), HOMO-1 → LUMO+2 (coeff = 0.1123), and HOMO → LUMO (coeff = −0.1708), which correspond to the observed onset of the absorption as shown in Figure 5a (409 and 299 nm) and to the two peaks which appear in the excited spectra as shown in Figure 6 (red line: 421 and 342 nm).

The TD-DFT calculation thus qualitatively predicts the Franck−Condon absorption and singlet manifold excitation energy gaps based on the ground-state geometry of the example cluster. The transition characteristics of the two excited states ES_1 (HOMO-2 → LUMO, HOMO → LUMO, and HOMO → LUMO+1) and ES_2 (HOMO-2 → LUMO, HOMO-1 → LUMO+2, and HOMO → LUMO) (calculated details are given in the Supporting Information) show that the occupied molecular orbitals (HOMO-2, HOMO-1, and the HOMO) possess prominent metal d character from six copper atoms combined with p character from the carbene carbon atoms, while the unoccupied molecular orbitals (LUMO, LUMO+1, and LUMO+2) possess mainly p and s character from six copper atoms and s character from the carbene carbon and p and s character from the bridged chlorine atoms. Thus, the two excitation or emission transition bands of cluster **2** can reasonably be assigned to the transitions from copper 3d to copper 4p or copper 3d, to copper 4s (3d → 4p or 3d →4s: metal−metal charge transfer MMCT) and copper 3d to carbene 2p or halide 3s and 3p (3d → 2p or 3d → 3s: metal to ligand charge transfer MLCT) (for the details of contribution from the molecular orbitals to the transition states see the Supporting Information). The TD-DFT calculation results show that the photophysical properties of these six-copper bridged carbene halide clusters arise from the core structure.

All previously reported copper cluster systems have highly symmetric geometries; Cu_4 is a tetrahedron,[21] and a previously reported Cu_6 case is an octahedron.[18] Herein we have found a rare example of a carbon-bridged, six-copper complex with an irregular boat-shaped core structure. In order to understand the assembly bonding details of these clusters, DFT calculations were performed with Gaussian-03.[22] The geometry optimization gave a minimum energy structure with Cu−Cu distances longer than those determined in the solid (see the Supporting Information); however, this is not too surprising, because the crystal structures are determined at higher temperatures and are also subject to intermolecular forces, whereas almost all of the calculations use isolated model structures. The principal structural feature is described as two seven-membered rings (C(1)−Cu(6)−Cl(2)−Cu(4)−N(4)−P(4)−C(2) or C(1)−P(3)−N(1)−Cu(1)−Cl(1)−Cu(5)−C(2)) and two five-membered rings (C(1)−P(2)−N(3)−Cu(3)−C(2) or C(1)−Cu(2)−N(2)−P(1)−C(2)) joined through the axis formed by two carbene carbons (C(1)- - -C(2)). Each copper(I) atom is coordinated with two atoms or a combination of three different atoms, combinations being C, X, N, C, or C, N (such as N(1)−Cu(1)−Cl(1), C(1)−Cu(2)−N(2), Cl(1)−Cu(5)−C(2), C(2)−Cu(3)−N(3), Cl(2)−Cu(4)−N(4), and Cl(2)−Cu(6)−C(1) in **2**) showing a nearly linear geometry with the bond angles of C−Cu−N, C−Cu−X and N−Cu−X in the range 169.21−174.22 which are close to 180° (see, as an example, the arrangement for **2** shown in Figure 8). The methyl or halide bridging and the PCP pincer ligand (N═P−C−P═N) cross-linking interactions bring three copper(I)−copper(I) pairs close with relatively short distances, indicating the existence of weak bonding, such as Cu(2)−Cu(3), Cu(1)−Cu(6), and Cu(4)−Cu(5) for **2** as shown in Figure 8.

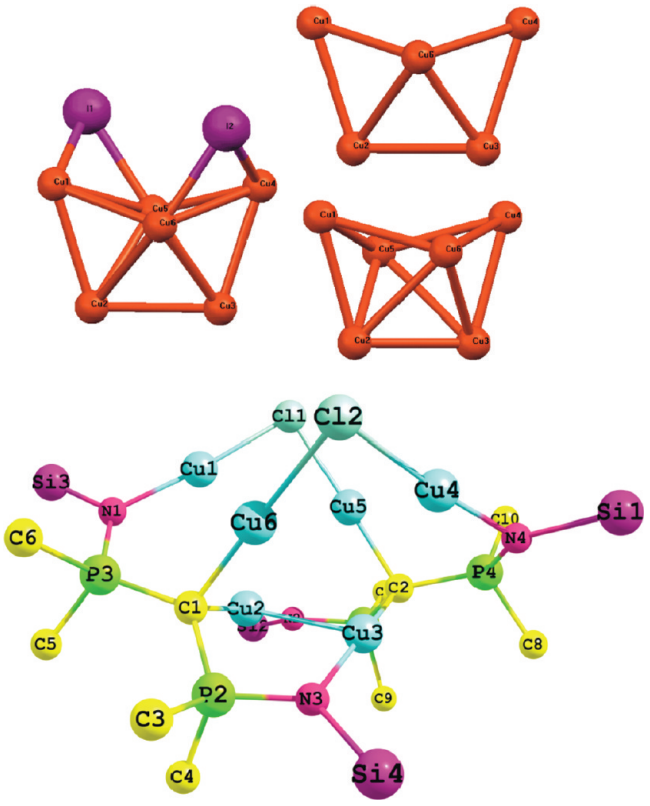

Figure 8. (top) Geometry of the six-copper cluster cores (**1**−**4**), with the core structure of complex **4** on the left and two views of the central core of the Cu_6 cluster on the right, the uppermost member being the symmetry of the cluster and the lower member being the boat shape of the cluster. (bottom) Optimized structure of cluster **2**.

The calculated molecular orbitals of **1** and **4**, which are representative of the methyl and one of the halide bridged complexes out of the group of the four clusters, are shown in Figures 9 and 10 (for **2** and **3** see the Supporting Information). As indicated by the calculated molecular coefficients, the strongest bonds between copper atoms within the cluster are mainly formed from s orbital overlap with very little d contribution. The methanediide bridging carbon atom bonds to the two different copper(I) atoms through its p_y and p_z atomic orbitals, forming a Cu−C−Cu bond angle close to 95° (see Figure 9, MO-184 and MO-185). The carbon to two copper bonds are 12.1% copper $s^{0.91}d^{0.09}$ and 87.9% carbon $s^{0.16}p^{0.84}$ and 11.8% copper $s^{0.93}p^{0.01}d^{0.06}$ and 88.2% carbon $s^{0.13}p^{0.87}$, as shown in NBO-148 and NBO-149, respectively, by the NBO analysis (Figure 11). The geometry optimized structure of **1** shows that the bond distances Cu(1)−Cu(6), Cu(4)−Cu(5), Cu(2)−Cu(3), Cu(1)−Cu(5), and Cu(4)−Cu(6) all decrease

(21) Raston, C. L.; White, A. H. *J. Chem. Soc., Dalton Trans.* **1976**, 2153–2156.

(22) (a) Frisch, M. J. et al. *Gaussian-03, Revision C02*; Gaussian, Inc., Pittsburgh, PA, 2004 (the full citation is given in the Supporting Information). (b) NBO component included in the Gaussian-03 program suite: Glendening, E. D.; Reed, A. E.; Carpenter, J. E.; Weinhold, F. *NBO version 3.1.*

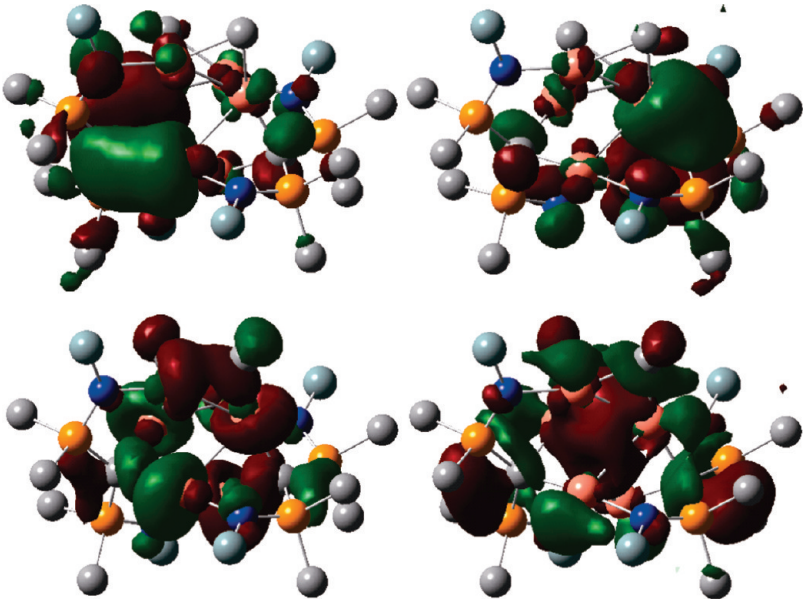

Figure 9. MO of cluster **1**: (top left) MO-184; (top right) MO-185; (bottom left) HOMO (MO-186); (bottom right) LUMO (MO-187).

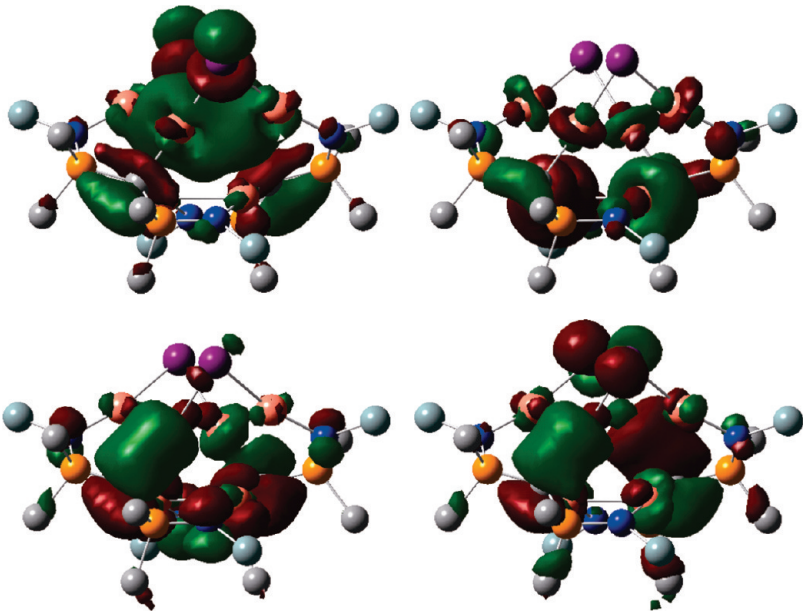

Figure 10. MO of cluster **4**: (top left) LUMO (MO-185); (top right) HOMO (MO-184); (bottom left) MO-183; (bottom right) MO-182.

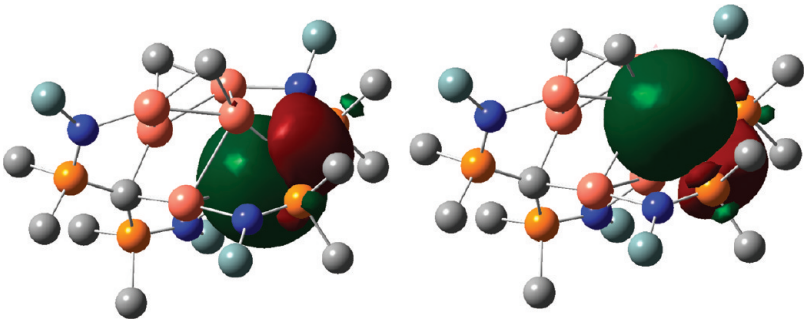

Figure 11. NBO of the key structure of the methanediide bridged carbon to two copper(I) atoms in cluster **1**: (left) NBO-148; (right) NBO-149.

gradually but fall within the usual Cu−Cu bonding distance, which is consistent with the crystal structure data. NBO analysis shows that the net bonding order of the three types of Cu−Cu bonding distances are, first, about 0.059 for both

Cu(1)−Cu(6) and Cu(4)−Cu(5) (calcd 2.632 Å) with a $s^{0.16}d^{0.84}$-(93.0%) and $s^{0.23}d^{0.77}$(7.0%) atomic orbital construction, second, 0.124 for Cu(2)−Cu(3) (calcd 2.565 Å) with $s^{0.95}p^{0.01}d^{0.04}$ (49.7%) and $s^{0.95}p^{0.01}d^{0.04}$ (50.3%) (approximately equal percentages of an almost pure s atomic orbital linkage) and, last, 0.180 for Cu(1)−Cu(5) and Cu(4)−Cu(6) (calcd 2.402 Å) with $s^{0.84}d^{0.16}$ (34.0%) and $s^{0.81}d^{0.19}$ (66.0%). The bond orders of all the connected copper pairs are relatively low, indicating that the interactions between these three types of copper pairs are relatively weak, and it is clear that the extensive additional bonding provided by the ligand contributes greatly to the stability of the system.

DFT calculations for the bimetallic complex **6** and the monometallic complex **7** were also performed with Gaussian-03.[22] The calculated molecular orbitals of these two complexes are presented in the Supporting Information. As indicated by the calculated molecular coefficients, the bimetallic copper complex showed multiple-bonding interactions between two copper atoms, the carbene center, and two P and two N atoms, which is very similar to our recently reported[6b] bimetallic palladium structure. The molecular coefficients and molecular orbitals for **6** and **7** are given in the Supporting Information. NBO analysis for **6** shows that the two carbon to copper bonds are 7.46% copper $s^{0.93}p^{0.02}d^{0.05}$ and 92.54% carbon $s^{0.18}p^{0.82}$ and 8.02% copper $s^{0.93}p^{0.02}d^{0.05}$ and 91.98% carbon $s^{0.19}p^{0.81}$ (as shown in NBO-77 and NBO-78, respectively, in the Supporting Information); hence, the bonding uses the same orbital components as cluster **1** but with lower copper and higher carbon contributions.

Conclusions

In conclusion, we have assembled a family of capped hexaatomic copper clusters with a unique nonsymmetric boat-type geometry supported by a pair of pincer methanediide (NPCPN) ligands which geminally bind to two copper atoms. The clusters are capped with methyl or halide ligands. Substitution reactions can be conducted on the capping ligands. This coordination geometry has not previously been reported. All clusters are fully characterized and quite stable in the solution, solid, and gas phases. These clusters are strongly photoluminescent in the solid state (with the solutions showing the same bands), and the absorption and emission wavelength values are dependent on the nature of the capping group ligand, indicating that the optical properties can be controlled by means of chemical alteration of the bridging groups. Two other complexes were also identified and characterized; a monocopper iodide complex and a bimetallic copper complex bridged by a spirocyclic carbon center. Both were fully characterized, including structural characterization. By comparisons of the copper cluster emission spectral properties to those of the monocopper complexes, we can verify that the tuning of the emission bands of the copper clusters to low energy, toward the visible region, with halide and methyl substitution is due to delocalized electrons within the clusters. DFT and NBO analysis has been conducted, as well as some preliminary reactivity studies. Further investigations on the catalytic reactivity and additional applications are proceeding.

Experimental Section

General Methods. All experimental manipulations were performed under rigorously anaerobic conditions using Schlenk techniques or in an argon-filled glovebox. The solvents used (special THF, toluene, and ether) were dried over appropriate drying agents and degassed by three freeze−pump−thaw cycles prior to use. The ^{1}H, ^{13}C, and ^{31}P NMR spectra were recorded on a Varian I400 spectrometer operating at 400.13, 100.6, and 161.9 MHz, respectively. The ^{1}H and ^{13}C NMR spectra were referenced internally using the residual proton solvent resonances, which were referenced to $SiMe_4$ (δ 0). ^{31}P NMR chemical shifts are given relative to an 85% H_3PO_4 external reference. UV−vis spectra were recorded with a Hewlett-Packard 8453 UV−vis DAD spectrophotometer. Photoluminescence (PL) spectra of single crystals in a sealed tube (**1**−**4**, **7**) were measured at room temperature using the 325 nm line of a He−Cd laser excitation source, and emission was detected with a fiber optic digital charge-coupled device (CCD) spectrometer whose spectral response was normalized using a standard blackbody radiator. Emission and excitation spectra in toluene were recorded using a Varian-Cary fluorescence spectrophotometer. Peak positions were determined by spectral deconvolution with ORIGIN. Quantum yields were obtained by comparing with Rhodamine-590 (QY = 0.95 in ethanol) dye in solution. Elemental analyses and IR spectra were carried out at the Analytical and Instrumentation Laboratory, Department of Chemistry, University of Alberta. The organolithium compounds $[Li_2L]_2$ (**1**) were prepared according to our published procedures.[23] The copper halides were purchased from either Strem or Aldrich; cod and all other precursors used were prepared by following or using procedures similar to those described in the literature.[24]

Synthetic Procedures. Synthesis of $[Cu_6\{C(Ph_2P{=}NSiMe_3)_2\}_2(CH_3)_2]$ (1). To a stirred THF (15 mL) suspension of $[NEt_4CuCl_2]$ (0.159 g, 0.6 mmol) was added, as a white solid, $[Li_2C(Ph_2P{=}NSiMe_3)_2]_2$ (0.115 g, 0.1 mmol). Then 0.125 mL (0.2 mmol) of 1.6 M $LiCH_3$, as an ether solution, was injected at room temperature. The reaction mixture turned bright yellow-green immediately after the injection. When the reaction was finished, the THF solvent was removed under vacuum and the remaining powder was washed with hexane and then dissolved in 10 mL of ether. The insoluble solid was coalesced by centrifugation. The clear yellow resultant solution was put inside a −20 °C freezer for a few hours. A yellow-green powder was collected and dried under vacuum to yield 0.134 g of yellow-green material (yield 88.0%). Crystals for X-ray diffraction were grown from THF solvent. IR data (Nujol mull): 3076 m, 3054 m, 2973 s, 2949 s, 2892 m, 2862 m, 1480 s, 1436 s, 1381 w, 1350 w, 1256 m, 1246 s, 1101 s, 1065 s, 1035 s, 915 w, 835 s, 780 s, 750 s, 739 s, 722 s, 713 m, 692 s, 672 m. ^{1}H NMR (toluene-d_8): δ 7.90 (m, phenyl, 4H), 7.78 (m, phenyl, 4H), 7.59 (m, phenyl, 4H), 7.50 (m, phenyl, 4H), 7.09 (m, phenyl, 8H), 6.98 (m, phenyl, 4H), 6.90 (m, phenyl, 4H), 6.69 (m, phenyl, 8H), 1.04 (s, −CH_3, 6H), 0.01 (s, −Si(CH_3)$_3$, 18H), −0.11 (s, −Si(CH_3)$_3$, 18H). ^{13}C{^{1}H} NMR (toluene-d_8): δ 135.92 (m, phenyl), 135.10 (m, phenyl), 132.94 (d, phenyl), 132.21 (d, phenyl), 131.95 (d, phenyl), 131.47 (d, phenyl), 129.69 (s, phenyl), 129.31 (s, phenyl), 4.86 (d, Si(*C*H$_3$)$_3$), 4.19 (d, Si(*C*H$_3$)$_3$), −18.99 (t, bridged −*C*H$_3$). ^{31}P{^{1}H} NMR (toluene-d_8): δ 25.14 (P_A) and 24.33 (P_B) ($^2J_{A-B}$ = 58.0 Hz). ESI-MS (THF + toluene): m/z 1524.0 $[M + H]^+$. Anal. Calcd for $C_{64}H_{82}N_4P_4Si_4Cu_6(C_4H_{10}O)_2$: C, 51.68; H, 6.15; N, 3.35. Found: C, 51.74; H, 6.18; N, 3.36. ^{1}H NMR in toluene-d_8 also detected the two ether solvent molecules quantitatively.

Synthesis of $[Cu_6\{C(Ph_2P{=}NSiMe_3)_2\}_2Cl_2]$ (2). To an ether (10 mL) suspension of $[(cod)_2Cu_2Cl_2]$ (0.124 g, 0.3 mmol) was added, as a white solid, $[Li_2C(Ph_2P{=}NSiMe_3)_2]_2$ (0.115 g, 0.1 mmol), and the mixture was stirred at room temperature for a few hours. The reaction mixture turned dark brown after 1 h and

(23) Kasani, A.; Babu, R. P. K.; McDonald, R.; Cavell, R. G. *Angew. Chem., Int. Ed.* **1999**, *38*, 1483–1484.

(24) (a) van den Hende, J. H.; Baird, W. C., Jr. *J. Am. Chem. Soc.* **1963**, *85*, 1009–1010. (b) Kok, J. M.; Skelton, B. W.; White, A. H. *J. Cluster Sci.* **2004**, *15* (3), 365–376. (c) Bowmaker, G. A.; Wang, J.-R.; Hart, R. D.; White, A. H.; Healy, P. C. *J. Chem. Soc., Dalton Trans.* **1992**, 787–795.

finally become a bright yellow-green solution. When the reaction was finished, insoluble solids were decanted by centrifugation. The clear yellow solution was kept inside a vial for a few days. The resultant bright yellow crystals were collected and dried under vacuum (yield 0.141 g (90.0%)). Crystals for X-ray diffraction were grown from ether solvent inside the NMR tube. IR data (Nujol mull): 3074 w, 3055 w, 2952 s, 2925 s, 2855 s, 1480 m, 1464 s, 1437 m, 1377 w, 1367 m, 1258 m, 1246 s, 1103 s, 1057 s, 1029 m, 1016 m, 841 s, 783 s, 740 s, 723 m, 714 w, 692 s, 674 m. ^{1}H NMR (THF-d_8): δ 8.00 (b, phenyl, 4H), 7.59 (q, phenyl, 4H), 7.44 (q, phenyl, 4H), 7.30 (m, phenyl, 8H), 7.12 (t, phenyl, 4H), 7.01 (m, phenyl, 8H), 6.88 (m, phenyl, 4H), 6.68 (b, phenyl, 4H), −0.36 (s, −Si(CH_3)$_3$, 18H), −0.41 (s, −Si(CH_3)$_3$, 18H). ^{13}C-{^{1}H,^{31}P} NMR (THF-d_8): δ 137.02 (s, phenyl), 136.15 (s, phenyl), 135.53 (s, phenyl), 134.29 (s, phenyl), 133.87 (s, phenyl), 133.21 (s, phenyl), 132.91 (s, phenyl), 132.45 (s, phenyl), 130.78 (s, phenyl), 130.73 (s, phenyl), 130.33 (s, phenyl), 130.20 (s, phenyl), 128.12 (s, phenyl), 128.03 (s, phenyl), 5.40 (s, −Si(*C*H$_3$)$_3$), 4.21 (s, −Si(*C*H$_3$)$_3$). ^{31}P{^{1}H} NMR (THF-d_8): δ 28.24 (P$_A$) and 26.17 (P$_B$) ($^2J_{A\text{-}B}$ = 56.0 Hz). ESI-MS (THF + toluene): m/z 1565.9 [M + H]$^+$. Anal. Calcd for $C_{62}H_{76}N_4P_4Si_4Cl_2Cu_6(C_4H_{10}O)_2$: C, 49.05; H, 5.61; N, 3.27. Found: C, 49.29; H, 5.68; N, 3.33. ^{1}H NMR in THF-d_8 also detected the two ether solvent molecules quantitatively.

Synthesis of [Cu$_6${C(Ph$_2$P═NSiMe$_3$)$_2$}$_2$Br$_2$] (3). To an ether (10 mL) suspension of [(cod)$_2$Cu$_2$Br$_2$] (0.150 g, 0.3 mmol) was added, as a white solid, [Li$_2$C(Ph$_2$P═NSiMe$_3$)$_2$]$_2$ (0.115 g, 0.1 mmol). The mixture was stirred at room temperature for 2 h. The reaction mixture turned bright yellow through time as the lithium salt was added. Insoluble solids were decanted by centrifugation. The clear yellow solution was kept in a vial for a few hours, and some white precipitate deposited on the bottom of the vial. The remaining clear solution was transferred to a new vial. After a few days, bright yellow crystals formed and they were collected and dried under vacuum (yield 0.119 g (72.0%)). Crystals for X-ray diffraction were grown from ether solvent inside the NMR tube. IR data (Nujol mull): 3073 m, 3048 m, 2951 s, 2895 s, 1481 m, 1436 s, 1398 w, 1307 w, 1246 s, 1180 w, 1101 s, 1061 s, 1028 m, 1010 m, 832 s, 785 s, 769 s, 741 m, 722 w, 692 s, 673 m. ^{1}H NMR (THF-d_8): δ 7.72 (m, phenyl, 8H), 7.58 (q, phenyl, 4H), 7.48(q, phenyl, 4H), 7.39 (m, phenyl, 4H), 7.32 (t, phenyl, 8H), 7.12 (m, phenyl, 4H), 7.01 (m, phenyl, 4H), 6.91 (m, phenyl, 4H), −0.26 (s, −Si(CH_3)$_3$, 18H), −0.30 (s, −Si(CH_3)$_3$, 18H). ^{13}C{^{1}H} NMR (THF-d_8): δ 136.82 (d, phenyl), 135.82 (d, phenyl), 133.83 (d, phenyl), 132.85 (d, phenyl), 132.54 (t, phenyl), 131.65 (s, phenyl), 130.80 (s, phenyl), 130.33 (d, phenyl), 129.20 (s, phenyl), 128.83 (t, phenyl), 128.09 (t, phenyl), 5.43 (d, Si(*C*H$_3$)$_3$), 4.26 (d, Si(*C*H$_3$)$_3$). ^{31}P{^{1}H} NMR (THF-d_8): δ 28.10 (P$_A$) and 26.59 (P$_B$) ($^2J_{A-B}$ = 57.0 Hz). ESI-MS (THF + toluene): m/z 1653.8 [M + H]$^+$. Anal. Calcd for $C_{62}H_{76}N_4P_4Si_4Br_2Cu_6$: C, 45.01; H, 4.60; N, 3.38. Found: C, 45.10; H, 4.63; N, 3.36.

Synthesis of [Cu$_6${C(Ph$_2$P═NSiMe$_3$)$_2$}$_2$I$_2$] (4). To an ether (10 mL) suspension of [(cod)$_2$Cu$_2$I$_2$] (0.178 g, 0.3 mmol) was added white solid [Li$_2$C(Ph$_2$P═NSiMe$_3$)$_2$]$_2$ (0.115 g, 0.1 mmol), and the mixture was stirred at room temperature for a few hours. The reaction mixture eventually turned yellow-orange. When the reaction was finished, the insoluble solid was decanted by centrifugation. The resultant clear yellow-orange solution was kept in a vial for a few days. Bright orange crystals deposited and were collected and dried under vacuum (yield 0.152 g (87.0%)). Crystals for X-ray diffraction were grown from ether solvent inside the NMR tube. IR data (Nujol mull): 3047 w, 2930 s, 2856 s, 1465 s, 1437 m, 1377 m, 1367 m, 1257 m, 1245 s, 1102 s, 1078 s, 1061 s, 1029 m, 832 s, 777 s, 751 s, 737 m, 713 m, 692 s, 672 m. ^{1}H NMR (THF-d_8): δ 7.77 (q, phenyl, 4H), 7.61 (q, phenyl, 4H), 7.52 (q, phenyl, 4H), 7.44 (m, phenyl, 4H), 7.36 (t, phenyl, 4H), 7.28 (t, phenyl, 4H), 7.13 (m, phenyl, 4H), 7.05 (m, phenyl, 4H), 6.98 (m, phenyl, 4H), 6.92 (m, phenyl, 8H), −0.22 (s, −Si(CH_3)$_3$, 18H), −0.29 (s, −Si(CH_3)$_3$, 18H). ^{13}C{^{1}H} NMR (THF-d_8): δ 138.05 (d, phenyl), 137.22 (d, phenyl), 136.84 (d, phenyl), 136.06 (d, phenyl), 135.62 (d, phenyl), 134.73 (d, phenyl), 134.06 (d, phenyl), 133.76 (d, phenyl), 133.26 (d, phenyl), 132.75 (q, phenyl), 130.84 (d, phenyl), 130.35 (d, phenyl), 129.13 (br, t, phenyl), 128.15 (m, phenyl), 5.43 (d, −Si(*C*H$_3$)$_3$), 4.34 (d, −Si(*C*H$_3$)$_3$). ^{31}P{^{1}H} NMR (THF-d_8): δ 28.95 (P$_A$) and 28.08 (P$_B$) ($^2J_{A-B}$ = 56.0 Hz). ESI-MS (THF+toluene): m/z 1747.8 [M+H]$^+$. Anal. Calcd for $C_{62}H_{76}N_4P_4Si_4I_2Cu_6\cdot{}^1/_2C_4H_{10}O$: C, 43.05; H, 4.57; N, 3.14. Found: C, 43.03; H, 4.55; N, 3.18.

Synthesis of [{(PPh$_3$)Cu}$_2$C(Ph$_2$P═NSiMe$_3$)$_2$] (6). To a yellow THF (10 mL) solution of [(NEt$_4$)Cu(PPh$_3$)Cl$_2$] (0.211 g, 0.4 mmol) was added solid [Li$_2$C(Ph$_2$P═NSiMe$_3$)$_2$]$_2$ (0.115 g, 0.1 mmol) with stirring at room temperature. The reaction mixture was then stirred at room temperature for 4 h to provide a light green solution. The THF solvent was removed under vacuum, and the remaining powder was dissolved in 10 mL of ether. The resultant insoluble solid was washed with toluene twice and decanted by centrifugation. The remaining combined solution was reduced to half of the volume under vacuum and put inside a −20 °C freezer for 2 days. A yellow-green powder was collected and dried under vacuum: 0.142 g of a yellow-green powder was obtained (yield 59.0%). IR data (Nujol mull): 3056 m, 3008 m, 2949 s, 2897 m, 2836 m, 1593 s, 1568 s, 1498 s, 1459 s, 1437 s, 1402 m, 1286 s, 1246 s, 1179 s, 1100 s, 1058 s, 1029 s, 935 s, 917 s, 830 s, 798 s, 784 m, 741 m, 729 m, 713 m, 693 s, 674 m. ^{1}H NMR (THF-d_8): δ 7.70−6.70 (m, phenyl, 50H), −0.578 (s, −Si(CH_3)$_3$, 18H). ^{13}C{^{1}H} NMR (THF-d_8): δ 141.71 (m, phenyl) 139.59 (d, phenyl), 135.10 (d, phenyl), 132.73 (t, phenyl), 130.40 (s, phenyl), 129.65 (s, phenyl), 129.35 (d, phenyl), 128.88 (d, phenyl), 127.40 (t, phenyl), 4.28 (s, Si(*C*H$_3$)$_3$). ^{31}P{^{1}H} NMR (THF-d_8): δ 4.06 (b), 19.34 (t, $^3J_{P-P}$ = 5.0 Hz). Anal. Calcd for $C_{67}H_{68}N_2P_4Si_2Cu_2$: C, 66.66; H, 5.63; N, 2.32. Found: C, 67.00; H, 5.70; N, 2.32.

Synthesis of [CuCH$_2$(Ph$_2$P═NSiMe$_3$)$_2$I] (7). Similar to the reaction conditions used for the preparation of **4** (Cu metal to ligand molar ratio at 6:1), about 10.0% of compound **7** was formed on the basis of ^{31}P NMR in solution. Two different colored crystals (a light green compound which proved to be [CuCH$_2$(Ph$_2$P═NSiMe$_3$)$_2$I$_2$] (**7**) and a red complex eventually identified as [Cu$_6$I$_2$C(Ph$_2$P═NSiMe$_3$)$_2$] (**4**)) were obtained from the reaction solution. When the copper to ligand molar ratio was increased to 10:1, the principal final isolated product was **7**. Thus, to an ether (10 mL) suspension of [(cod)$_2$Cu$_2$I$_2$] (0.300 g, 0.5 mmol) was added [Li$_2$C(Ph$_2$P═NSiMe$_3$)$_2$]$_2$ (0.115 g, 0.1 mmol) as a white solid, and the mixture was stirred at room temperature for a few hours. The reaction mixture eventually yielded a yellow-orange solution. When the reaction was finished, insoluble solids were decanted by centrifugation. The clear yellow-orange solution was kept inside the vial for a few days. Slightly yellow-green crystals were collected and dried under vacuum (yield 0.117 g (78.0%)). Crystals for X-ray diffraction were grown from ether solvent inside an NMR tube. IR data (Nujol mull): 3054 w, 2965 s, 2950 s, 2885 s, 2854 s, 2812 w, 1620 m, 1487 s, 1435 m, 1363 m, 1338 m, 1242 m, 1180 s, 1113 s, 1045 w, 1025 w, 999 m, 841 s, 791 s, 779 s, 759 m, 749 m, 709s, 692 m, 662 m. ^{1}H NMR (THF-d_8): δ 7.72 (t, phenyl, 8H), 7.38 (m, phenyl, 4H), 7.29 (m, phenyl, 8H), 3.8 (b, −CH$_2$−, 2H), −0.25 (s, −Si(CH_3)$_3$, 18H). ^{13}C{^{1}H,^{13}P} NMR (THF-d_8): δ 132.08 (s, phenyl), 131.51 (s, phenyl), 127.43 (s, phenyl), 50.00 (br, −CH$_2$−), 3.33 (s, -Si(*C*H$_3$)$_3$). ^{31}P{^{1}H} NMR (THF-d_8): δ 12.7 (broad peak). Anal. Calcd for $C_{31}H_{40}N_2P_2Si_2ICu(C_4H_{10}O)$: C, 51.06; H, 6.08; N, 3.40. Found: C, 51.22; H, 5.95; N, 3.47. ^{1}H NMR in THF-d_8 also detected the ether solvent molecule quantitatively.

Crystal Structure Determination. Suitable crystals of **1**−**4**, **6**, and **7** were mounted on glass fibers by means of mineral oil, and data were collected using graphite-monochromated Mo Kα radiation (0.710 73 Å) on a Bruker D8/APEX II CCD diffractometer. The structures were solved by direct methods using SHELXL-97[25] and refined using full-matrix least squares on

(25) Sheldrick, G. M. *Acta Crystallogr.* **2008**, *A64*, 112–122.

F^2 (SHELXL-97).[26] All of the non-hydrogen atoms in the structure were refined with anisotropic displacement parameters. Selected crystal data and structure refinement details for all the compounds are given in Table 3.

Computational Details. The geometric optimizations of some selected core structures were performed with the Gaussian03 program[22] using the density functional theory (DFT) method. The Becke three-parameter hybrid functional with the Lee−Yang−Parr[27] correlation functional (B3LYP)[28] was employed for all calculations. Gaussian NBO analysis was carried out for the final optimized structures.[22] The LanL2DZ basis set on Cu and halides and the 6-31G(d) basis set on Si, P, N, C, and H were used for all the calculations. In order to save computing time, models were used in which the outside phenyl ring was replaced with methyl groups and original methyl groups were replaced with H, except in the calculation of **1**, where the methyl groups on Si were retained. Also, one calculation for **4** was done with the complete molecular structure including phenyl substituents (see the Supporting Information).

(26) Sheldrick, G. M. *SHELXL-97: Program for Crystal Structure Determination*; University of Göttingen, Göttingen, Germany, 1997.
(27) Lee, C.; Yang, W.; Parr, R. G. *Phys. Rev. B* **1988**, *37*, 785–789.
(28) Becke, A. D. *J. Chem. Phys.* **1993**, *98*, 5648–5642.

Acknowledgment. We thank the Natural Sciences and Engineering Research Council of Canada and the University of Alberta for financial support. We also thank the University of Alberta for supporting the X-ray Crystallography, NMR and Analytical and Instrumentation laboratories at the Department of Chemistry. We thank José Rodriguez-Nunez and Lydia Glover (University of Alberta) for assistance with measurements of the photoluminescence spectra (PL) and Profs. Al Meldrum (Physics, University of Alberta) and Jonathan G. C. Veinot (Chemistry, University of Alberta) for access to the solid and solution PL spectrometers.

Supporting Information Available: For **1**−**4**, **6**, and **7**, CIF files giving atomic positions and displacement parameters, anisotropic displacement parameters, bond lengths, and bond angles, figures giving mass spectra, NMR spectra, and TGA analyses, and tables of crystal data, computed OPT structures, molecular orbitals, and NBO, as well as details of TD-DFT. This material is available free of charge via the Internet at http://pubs.acs.org.